VIBRATION REDUCTION BY TUNED MASS DAMPERS INSIDE CAVITIES OF TOPOLOGY OPTIMIZED LATTICE STRUCTURES

Janousek, Marc Konrad Bernd;
Xu, Duo;
Vazhapilli Sureshbabu, Anand;
Zimmermann, Markus

Techische Universität München

ABSTRACT

Tuned mass dampers may be used to improve vibrational behavior of structures. However, they require space to move. This paper presents an approach to incorporate tuned mass dampers into a lightweight-optimized structure without extra space requirement. It is based on (1) topology optimization (TopOpt) with unit cells and (2) vibration reduction with multiple tuned mass dampers (m-TMD) within the unit cells. The topology optimization is performed with a physics-informed penalty factor, unique to the chosen unit cell. Subsequently, the weight optimal density distribution is realized by populating the design domain with unit cells of ten different densities. To reduce the induced vibration, m-TMDs are placed inside the cavities of the unit cells in the grey scale regions. The effectiveness of the approach is demonstrated for the design of a 2-segment robot arm. The resulting unit cell robotic arm (UC-Arm) is 3.6% lighter than the reference model, maintains the same static performance, and shows a 60% smaller dynamic displacement in the observed frequency range. No extra space is required for the motion of the m-TMD.

Keywords: Optimisation, 3D printing, Lightweight design

Contact:
Janousek, Marc Konrad Bernd
Techische Universität München
Germany
marc.janousek@me.com

Cite this article: Janousek, M. K. B., Xu, D., Vazhapilli Sureshbabu, A., Zimmermann, M. (2023) 'Vibration Reduction by Tuned Mass Dampers Inside Cavities of Topology Optimized Lattice Structures', in *Proceedings of the International Conference on Engineering Design (ICED23),* Bordeaux, France, 24-28 July 2023. DOI:10.1017/pds.2023.380

1 INTRODUCTION

Functional robotic arms with rigid linkages have complicated dynamic characteristics. It is a complex distributed parameter system with infinite dimensions and non-linearity. Due to their elastic behavior, these robot arms may be difficult to position and control properly. Another thing to keep in mind when building such robot arms is that they need to be light to require little power and torque. One approach for lightweight design in such systems is topology optimization. Utilizing composite sandwich or lattice structures is another strategy for lightweight architecture. Lattice structures, also known as unit-cell lattices, are frequently employed in lightweight structural designs and multi-functional applications due to their wide range of design feasibility and minimal complexity in behavior modeling

By using unit-cells to take advantage of grey-scale effects, i.e., the combination of these two techniques, *topology optimization with unit-cells* improves the stiffness-to-weight ratio of arbitrary parts. These effects were for example investigated by Sigmund *et al.*, 2016, where the authors concluded that the weight-optimal design delivered by SIMP optimization (Bendsøe und Sigmund, 2004) includes areas with intermediate material properties. These areas arise because of the design variable called “density”. The density influences all material properties of one FEM element like:

$$Property_{Element} = Property_{Solid} * Density \quad (1)$$

Elements that have a density between one and zero are referred to as "grey elements". This is due to the fact that they have properties halfway between a solid, which is frequently depicted in black, and a void, which is frequently depicted in white. With the advent of 3D printing, the concept of using unit-cells to improve part performance gained traction since the intermediate material qualities offered by grey areas could not be produced using classic subtractive manufacturing methods. Subsequently, many approaches have been introduced aiming to exploit this effect meaningfully. For example, Han und Lu, 2018, changed the size of the unit-cells while keeping the cross-sections constant. Zheng *et al.*, 2021 used a spinodoid material which allowed for a seamless change of material properties. Wang *et al.*, 2020 used a set of unit-cells that not only differed in volume density but also had varying features. One approach that stands out among all the others due to its promising results in experiments and simulations was the four steps workflow introduced by Zhang *et al.*, 2021, shown in Figure 1.

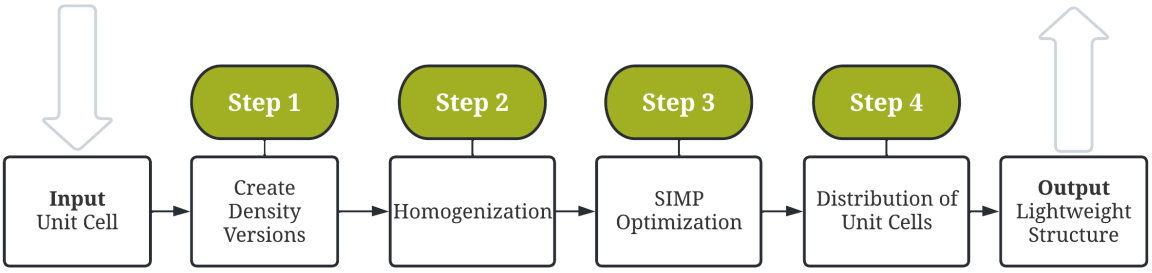

Figure 1. Four steps workflow to enhance any topology optimization based on SIMP for the application of unit-cells

In the first stage, eleven unit cell designs with different densities, ranging from 0% to 100% with 10% increments, are constructed for an initial unit-cell. In the second stage, homogenization simulations are used to derive the material properties for those eleven volume density variations. In stage three SIMP topology optimization, the physics-based penalty function will be employed to approximate the relationship between Young's modulus and volume density. The weight optimal unit-cell volume density distribution, which will be then used to model the unit-cells in the design domain in step four, is calculated through this optimization. In this study, two structures were optimized, and they were compared with their conventionally optimized counterparts. The demonstrated performance improvements ranged from 118% to 7%, demonstrating a considerable dependence on the structure and the load case.

Since stiffness in regions not subject to stress during the load case(s) of interest must be sacrificed to reduce weight, components may become globally less rigid, decreasing their eigenfrequencies. This

https://doi.org/10.1017/pds.2023.380 Published online by Cambridge University Press

creates the prospect that the shifted eigenfrequencies are now dangerously near to the excitation frequencies of oscillating external forces. If true, this leads to significant oscillations and a decrease in lifetime brought on by outside influences that did not affect the non-lightweight structure negatively. To prevent this adverse effect from happening, tuned mass dampers (TMD) can be deployed in these structures.

A single TMD can only dampen one specific frequency, however, a whole frequency range can be dampened by adding multiple tuned mass dampers (m-TMD) with adjacent frequencies into the system. This elongation of stopbands across frequency ranges is what the field of *vibration reduction with m-TMDs* deals with. A demonstration is shown in Neighborgall *et al.*, 2020 where 40 TMDs made from fettuccini pasta are used to design the frequency response function (FRF) of a structure with two primary masses in a two-story configuration. In both simulation and experiment, the effect of the m-TMDs on the FRF was shown by a lowering of the amplitude around the two eigenfrequencies. Many examples exist with even higher numbers of m-TMDs. Claeys *et al.*, 2017 dampened the FRF of a rectangular tube with 640 unit-cell TMDs, Sangiuliano *et al.*, 2019 improved the NVH behavior of a car by replacing the rear shock towers with 105 TMDs and Sangiuliano *et al.*, 2018 dampened a 2D structure with 88 unit-cell TMDs.

In this paper, the benefits of these two mentioned fields are combined to design lightweight components which do not struggle with induced vibration due to their structurally designed frequency response. This is achieved in two steps: A) Calculating the weight optimal unit-cell distribution with an adapted version of informed decomposition (Krischer und Zimmermann, 2021) which has been enhanced to treat unit-cells according to Zhang *et al.*, 2021. B) Adding m-TMDs into the internal cavities of the unit-cell to iteratively adapt the dynamic response. The proposed method is illustrated by improving an existing two-component robotic arm designed with informed decomposition.

The paper is structured as follows: Before going into all the necessary design strategies to meet the static and dynamic load requirements, Section 2 explains the design challenge at hand. The findings of comparing the discovered design to a conventionally optimized part in simulation are discussed in section 3 of the paper. Section 4 draws conclusions, identifies drawbacks, and suggests possible next steps.

2 TOP-DOWN DESIGN OF A ROBOTIC ARM

2.1 Design task definition

The upper and lower arms, which together make up the robotic arm, have measurements of 180 x 80 x 60 mm. The assembly has a total of two degrees of freedom due to the joint that connects the upper arm to a hard connection on one end and the lower arm on the other. An attachment interface at the lower arm's tip allows for the application of external forces.

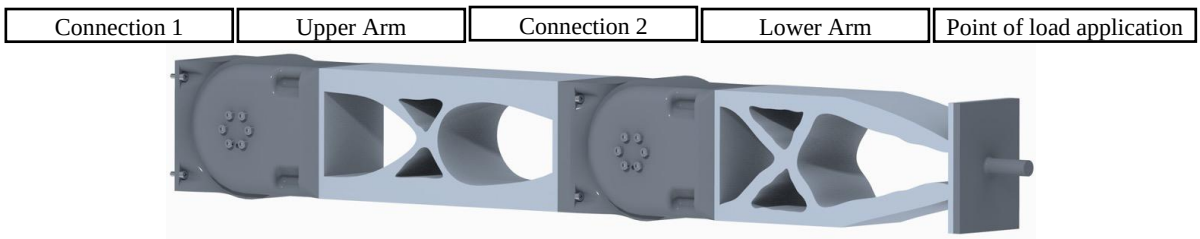

Figure 2. Two-component robotic arm designed with informed decomposition, with the name of each component shown above.

The robotic arm structure shown in Figure 2 is designed with informed decomposition (Krischer und Zimmermann, 2021). Due to its capability to identify the weight optimal design for each component in a multi-component system, this method was selected. The procedure can consider a static stiffness constraint in addition to the design space size and material characteristics, which in this case is:

- A static load of 2.5 kg is applied in a fully stretched-out configuration at the tip, where the maximal permitted tip displacement is 0.25 mm

It is uncertain if the discovered design can offer enough dynamic stiffness to prevent oscillations since in this instance, the informed decomposition only considers static stresses. This is challenging since the robotic arm also needs to meet a requirement for dynamic load, namely:

https://doi.org/10.1017/pds.2023.380 Published online by Cambridge University Press

- A dynamic load of 1 kg applied in a fully stretched-out configuration, the load can oscillate in a frequency range between 0 Hz and 150 Hz, and the maximum allowed end deflection is 1.25 mm.

A methodology that can consider both static and dynamic requirements, necessary to develop a better robotic arm. The next section will describe one such workflow. If successful, the discovered designs will be evaluated in simulations against the reference design with SIMSOLID® (SIMSOLID) using the SLA resin material TOUGH1500 with the Young's modulus of 981 N/mm^2, which is the experimentally derived Young's Modulus of a 3D-printable material out of which the robotic arms will be manufactured. This material was chosen since it provides high strength, and high durability, and the fact that SLA 3D printing brings about highly accurate manufacturing. Both mentioned requirements are not based on any specific application. However, since these can be adapted to any specific application, the method proposed in this paper is valid in general.

2.2 Design for the static load case

Five steps will be taken to combine topology optimization with unit-cells and vibration reduction using multiple-tuned mass dampers (m-TMD). The lattice grid that will be filled with m-TMDs is initially created in the first four steps, which are depicted in Figure 3. A further advantage of this design approach is that it distinguishes between static requirements (steps one through four) and dynamic requirements (step five). A detailed explanation of the design process is explained in the form of an Extended Design Structure Matrix (XDSM) below:

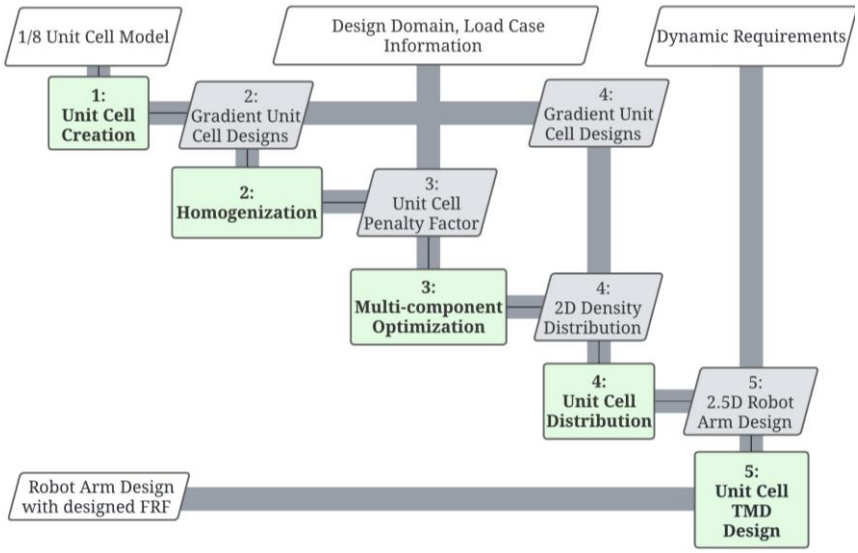

Figure 3. XDSM of the design for a static load case

The first required input is a 1/8 model of the unit-cell that shall be used for the component design. For the case at hand, this unit-cell will be a simple cube, from now on referred to as sCube, see Figure 4.

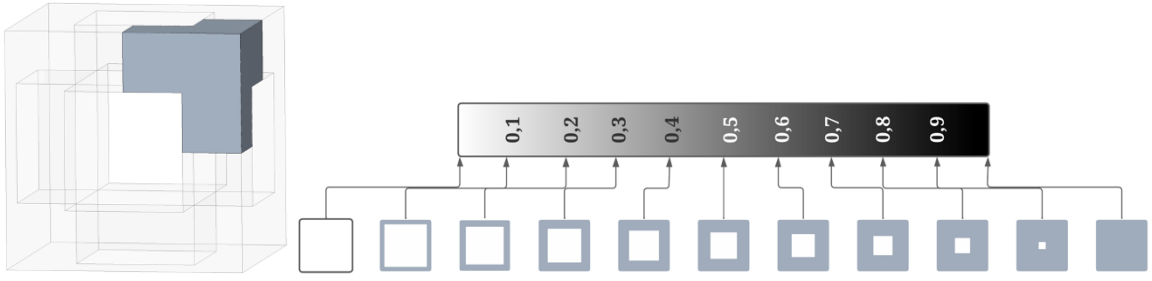

Figure 4. sCube unit-cell in opaque with a 1/8 as solid (left), used sCube volume density version during the design of the robotic arm (right)

The next stage is to generate various volume density variations of this simple cube unit-cell. Figure 4 illustrates the eleven versions that are required, with relative densities ranging from 0% to 100% in 10% increments.

https://doi.org/10.1017/pds.2023.380 Published online by Cambridge University Press

In step 4, "Unit-cell Distribution," which is published in the STL file format, the 1/1 or "full" versions of these unit-cells will be used, but step 2, "Homogenization," which is presented in the STEP file format, will still use the 1/8 version. In step 2, a customized version of the ABAQUS® Plug-in "easyPBC" (SL *et al.*) is used to derive the relationship between the unit-cell volume density and its Young's modulus. Next, this relationship is approximated by a function that will be used as a physics-informed penalty function during the informed decomposition. For the unit-cell sCube, this approximated physics-informed penalty function comes out to be:

$$f(\rho) = \rho^{1.78} \tag{2}$$

Figure 5 demonstrates how well this function, particularly in the higher-volume-density regions, matches the simulated Young's moduli. The strength of the unit-cell is slightly undervalued in the lower-volume-density areas, which is acceptable for the current task.

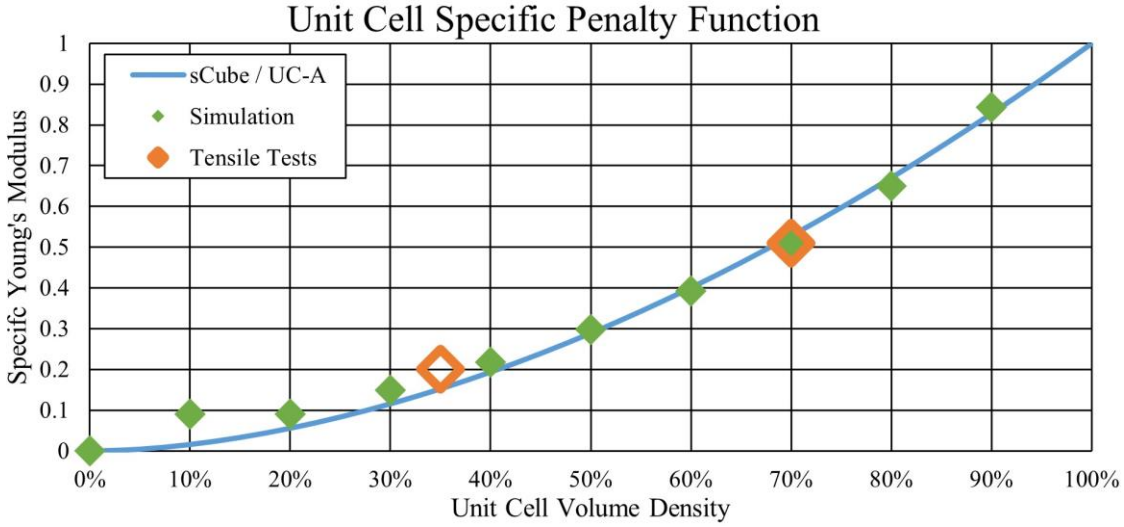

Figure 5. The unit-cell-specific penalty function of the sCube compared to the relative Young's modulus for different densities derived through A, simulation and B, tensile tests

In addition to the simulation results and the physics-informed penalty function, Figure 5 shows the results of tensile testing for two sCube densities. For the densities 35 % and 70 % the relative Young's Modulus was measured on E DIN 50125:2021-08 samples with a total length of 120 mm. The difference between the measured and simulated relative Young's moduli was less than 2%, demonstrating the simulation's validity.

The informed decomposition can be modified to determine unit-cell volume density rather than material density once the unit-cell-specific penalty factor is at hand. As a result, the workflow's penalty value is altered to the derived 1.78, which is unique to the sCube unit-cell. Figure 6 shows the 2.5D design of the unit-cell robotic arm (UC-A) without m-TMDS. The following 4 mm sized unit-cells are distributed inside the design domain in accordance with the computed unit-cell volume density distribution.

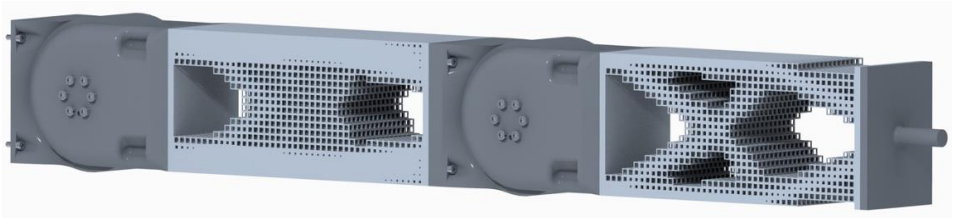

Figure 6. Unit-cell robotic arm without m-TMDS

2.3 Design for the dynamic load case

The FRF of the initial robotic arm design minus the m-TMDs is calculated in step five, which is an iterative workflow. The first step of each iteration is the calculation of the FRF of the current design in SIMSOLID (SIMSOLID). If the maximum system oscillation surpasses the defined limit, m-TMDs

https://doi.org/10.1017/pds.2023.380 Published online by Cambridge University Press

are added into the system with an eigenfrequency matching the frequency of the highest maximum system oscillation The total number of unit-cell TMDs added in one iteration varies between 500 and 2400 and is depending on the amplitude of the FRF peak. This figure is so high because one unit-cell TMD must be small enough to fit inside of one unit cell, and as a result, only makes up 0.00104% of the mass of the bare UC-Arm. Only unit-cells with a volume density of 40% or lower have sufficient interior space to contain an m-TMD, even when they are this compact. Figure 7 shows the finished 2.5D UC-Arm design, which was enhanced by the addition of 8160-unit-cell TMDs. The magnified cutout in Figure 7 aims at showing the spherical masses of the TMDs as well as the circular rod which connects them to the arm structure.

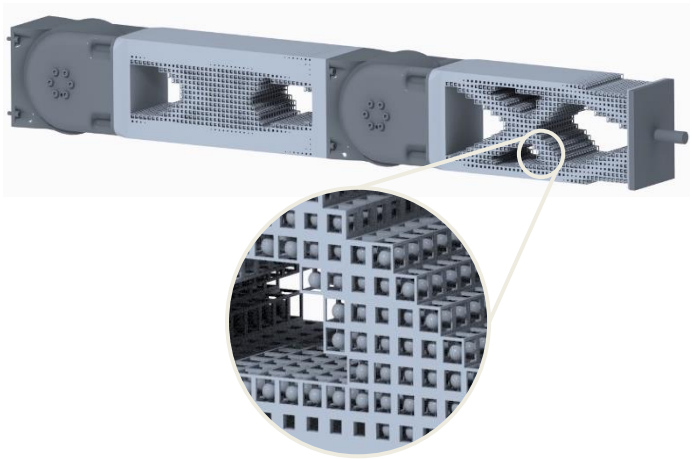

Figure 7. Unit-cell robotic arm with m-TMDS

3 SIMULATION RESULTS & DISCUSSION

In this section, the performance of three iteratively enhanced robotic arm designs is compared:

- The reference robot arm designed with informed decomposition
- The unit-cell robot arm design without m-TMDs and
- The unit-cell robot arm with m-TMDs to tune its FRF.

The focus is initially on the sCube unit-cell's micro-level performance before the macro-level performance is explored. Its performance must be understood to make the proper inferences later because it is utilized in the construction of the two unit-cell robotic arms.

3.1 Micro-level performance

First, a measurement must be found based on which the sCube can be judged. Since the most common goal behind unit-cell design is lightweight, a good unit-cell is one with a high specific stiffness and minimal weight. In lightweight design, this is one of the most important measurements and it is typically judged by comparison with the upper Hashin-Shriktman bound (HS-Bound) (Hashin und Shtrikman, 1963). This bound is the theoretical limit for a unit-cell specific Young's modulus assuming isotropy. Figure 8 shows a comparison between A, the upper HS-Bound, and B, the unit-cell-specific penalty factor of the sCube.

https://doi.org/10.1017/pds.2023.380 Published online by Cambridge University Press

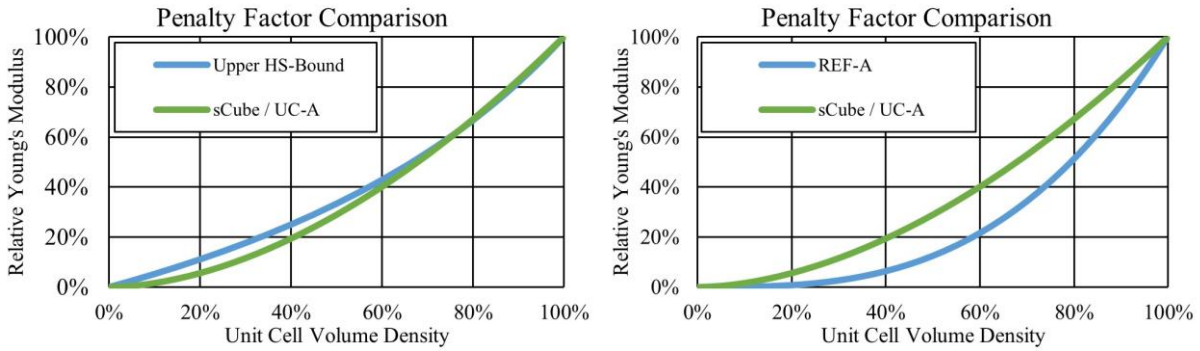

Figure 8. Comparison between the penalty function of the sCube and the upper Hashin-Shriktman Bound (left) and the comparison between the penalty function used in the design of the three discussed robotic arms (right).

The sCube is a good lightweight unit-cell, as shown by a comparison between its penalty function and that of the higher HS-Bound. This is due to the proximity of the two functions across the full spectrum of unit-cell densities, particularly in higher-volume-density areas. The sCube unit-cell is highly suited for this application for several reasons, including its good stiffness-to-weight ratio. The fact that it does not produce closed internal spaces, which facilitates resin-based 3D printing and its subsequent drainage and efficient curing, making it easier to build than plate lattices, which have greater lightweight potential. When compared to unit-cells from other studies, the sCube unit-cell offers large internal cavities to accommodate m-TMDs, making it an exceptionally useful feature incorporated in this design.

The second comparison of penalty factors compares the sCube's unit-cell-specific penalty factor, A, with the reference robot arm's penalty value, B. It is conceivable that employing the sCube unit-cell will result in a weight reduction while preserving stiffness because its penalty factor outperforms that of the Ref-A. The purpose of the following section is to examine the accuracy of this claim.

3.2 Static load case

The statement from the previous section can be divided into two parts: A, The unit-cell robotic arms must be lighter than the reference, and B, The unit-cell robotic arms must be similarly stiff. Figure 9 compares the weights of the three robotic arms to verify the first part of this claim.

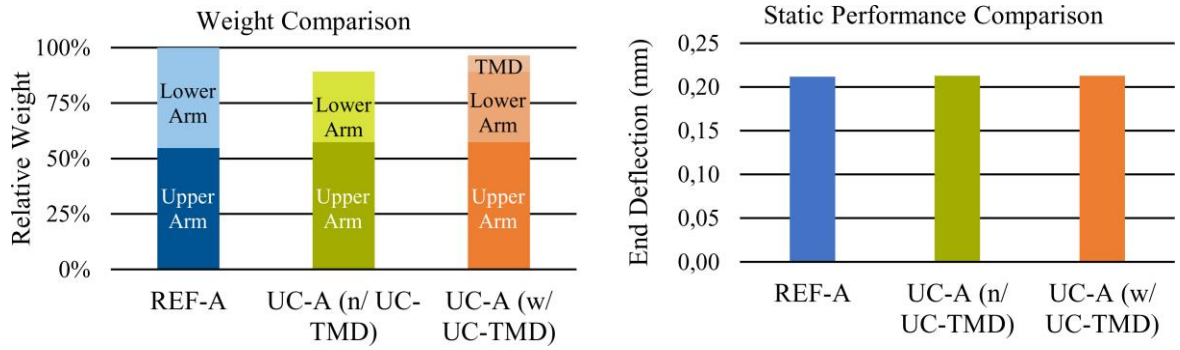

Figure 9. Weight comparison between the three discussed robotic arms (left) and comparison of the end deflection between the three discussed robotic arms (right)

The Ref-A is the heaviest of them all, followed by the UC-A with unit-cell TMDs which is 3.6 % lighter, and the unit-cell arm without the unit-cell TMDs which weighs 10.8 % less than the reference arm. This implies that the first part of the hypothesis is accurate. This suggests that the initial portion of the assertion is accurate. By simulating the static load case and contrasting the end deflections in Figure 10, the second part is also validated. When a force of 2.5 kg is applied, the tip displacement of the three robotic arms is around 0.21 mm. This indicates that all three robotic arm designs satisfy the static load stiffness requirement, which demanded the maximum displacement to be less than 0.25 mm.

https://doi.org/10.1017/pds.2023.380 Published online by Cambridge University Press

3.3 Dynamic load case

Proceeding to the dynamic load requirement, where it is specified that if a force of 1 kg is applied with a frequency between 0 Hz and 150 Hz, the greatest endpoint deflection must remain below 1.25 mm. Figure 10 displays the FRF in the frequency range to evaluate the three robotic arm's compliance with this requirement and assess their performance.

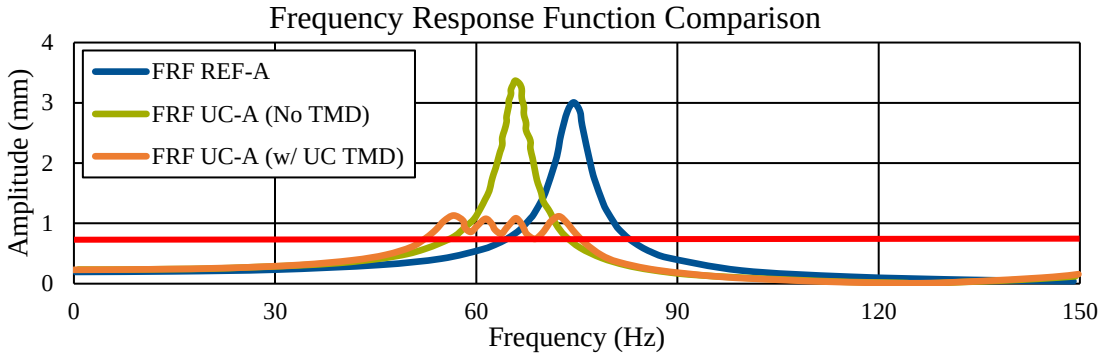

Figure 10. Comparison of the FRF between the three discussed robotic arms, with the permitted amplitude shown as a red line

The figure demonstrates that an eigenfrequency that appears to be in the frequency range of interest is present for both the unit-cell arm without TMDs and the reference robotic arm. This results in significant oscillations in both cases, preventing both robotic arms from achieving the target minimum displacement.

The third robotic arm meets the dynamic requirements due to the m-TMDs that reduce the effects of the eigenfrequency. The eigenfrequency peak is divided into four local maxima by the 8160's m-TMDs, none of which can induce oscillations that are greater than the allowed 1.25 mm. The division of one large peak into several smaller ones is a typical behavior for TMD-tuned systems. A TMD always introduces an additional degree of freedom into the system which brings about an additional eigenfrequency. According to the simulations, each m-TMD has an oscillatory displacement that is no higher than 1.7mm. The simulation data shows that this satisfies the maximum permissible displacement of 1.83 mm because the m-TMDs must always stay inside the unit-cell to prevent obstructing the design space.

4 CONCLUSION

The study's findings demonstrate that the suggested workflow can make use of unit-cell m-TMDs in a way that: a) it decouples static and dynamic system requirements, making them independently treatable during component design; and b) generates designs with comparable weight and static load performance but noticeably better dynamic load performance, as Table 1 shows.

Table 1: Summarisation of robotic arm performance

Robot Arm	Static End Deflection (in mm)	Static Requirement met	Max. Dynamic Oscillation (in mm)	Dynamic Requirement met
REF-A	0.21	Yes	3.00	No
UC-A (no TMD)	0.21	Yes	3.37	No
UC-A (w/ UC TMD)	0.21	Yes	1.31	Yes

Since no additional design space is required, this method is a viable solution for weight-optimizing specific components of existing components and assemblies. Since unit-cell designs are infamous for performing differently in experiments than they do in simulations due to manufacturing and material inefficiencies (Zhang *et al.*, 2021), experimental verification of the simulation results is still necessary but challenging. Additionally, it is often not physically feasible to manufacture components with this

https://doi.org/10.1017/pds.2023.380 Published online by Cambridge University Press

level of accuracy using additive manufacturing procedures which either require a lot of post-processing or have errors caused by material behavior. The performance decline may also be caused by manufacturing errors, which could be problematic for m-TMDs. High-precision manufacturing is essential for these designs since even the slightest difference in the m-TMD dimensions could cause noticeable changes in the eigenfrequency. If the m-TMDs' eigenfrequency does not match the system's eigenfrequency, they may lose some or all their influence on the system's FRF.
Future investigation into this topic will focus on the 3D printing of unit-cell structures, incorporating manufacturing viability into the approach, identifying the key restrictions, optimizing the unit-cell design for them, and evaluating the costs-to-benefit relationship.

REFERENCES

Bendsøe, M. P. and Sigmund, O. (2004), *Topology Optimization*, Springer Berlin Heidelberg, Berlin, Heidelberg.

Claeys, C., Rocha de Melo Filho, N. G., van Belle, L., Deckers, E. and Desmet, W. (2017), "Design and validation of metamaterials for multiple structural stop bands in waveguides", *Extreme Mechanics Letters*, 12. Jg., S. 7–22.

Han, Y. and Lu, W. F. (2018), "A Novel Design Method for Nonuniform Lattice Structures Based on Topology Optimization", *Journal of Mechanical Design*, 140. Jg., Nr. 9.

Hashin, Z. and Shtrikman, S. (1963), "A variational approach to the theory of the elastic behaviour of multiphase materials", *Journal of the Mechanics and Physics of Solids*, 11. Jg., Nr. 2, S. 127–140.

Krischer, L. and Zimmermann, M. (2021), "Decomposition and optimization of linear structures using meta models", *Structural and Multidisciplinary Optimization*, 64. Jg., Nr. 4, S. 2393–2407.

Neighborgall, C. R., Kothari, K., Sriram Malladi, V. V. N., Tarazaga, P., Paruchuri, S. T. and Kurdila, A. (2020), "Shaping the Frequency Response Function (FRF) of a Multi-Degree-of-Freedom (MDOF) Structure Using Arrays of Tuned Vibration Absorbers (TVA)", in Mains, M. L. and Dilworth, B. J. (Hg.), *Topics in Modal Analysis & Testing, Volume 8, Conference Proceedings of the Society for Experimental Mechanics Series*, Springer International Publishing, Cham, S. 317–326.

Sangiuliano, L., Claeys, C., Deckers, E., Pluymers, B. and Desmet, W. (2018), "Force Isolation by Locally Resonant Metamaterials to Reduce NVH", in *SAE Technical Paper Series, JUN. 20*, 2018, SAE International400 Commonwealth Drive, Warrendale, PA, United States.

Sangiuliano, L., Claeys, C., Deckers, E., Smet, J. de, Pluymers, B. and Desmet, W. (2019), "Reducing Vehicle Interior NVH by Means of Locally Resonant Metamaterial Patches on Rear Shock Towers", in *SAE Technical Paper Series, JUN. 10*, 2019, SAE International400 Commonwealth Drive, Warrendale, PA, United States.

Sigmund, O., Aage, N. and Andreassen, E. (2016), "On the (non-)optimality of Michell structures", *Structural and Multidisciplinary Optimization*, 54. Jg., Nr. 2, S. 361–373.

SIMSOLID, verfügbar unter https://www.altair.com/simsolid/.

SL, O., PD, D. and S. Sriramula, "Development of an abaqus plugin tool for periodic rve homogenisation", *Engineering with Computers*, 2019. Jg., Nr. 35, S. 567–577.

Wang, C., Gu, X., Zhu, J., Zhou, H., Li, S. and Zhang, W. (2020), "Concurrent design of hierarchical structures with three-dimensional parameterized lattice microstructures for additive manufacturing", *Structural and Multidisciplinary Optimization*, 61. Jg., Nr. 3, S. 869–894.

Zhang, J., Sato, Y. and Yanagimoto, J. (2021), "Homogenization-based topology optimization integrated with elastically isotropic lattices for additive manufacturing of ultralight and ultrastiff structures", *CIRP Annals*, 70. Jg., Nr. 1, S. 111–114.

Zheng, L., Kumar, S. and Kochmann, D. M. (2021), "Data-driven topology optimization of spinodoid metamaterials with seamlessly tunable anisotropy", *Computer Methods in Applied Mechanics and Engineering*, 383. Jg., Nr. 9, S. 113894. http://doi.org/10.1016/j.cma.2021.113894

https://doi.org/10.1017/pds.2023.380 Published online by Cambridge University Press

CAMBRIDGE
UNIVERSITY PRESS